UNCONVENTIONAL RESOURCES TECHNOLOGY CONFERENCE
FUELED BY SPE • AAPG • SEG

URTeC: 4042576

Modeling of Proppant Flowback to Quantify and Predict its Impact on Shale Gas Production under Different Drawdown Strategies – A Vaca Muerta Case Study

Agustin G. Garbino*[1], D. Nicolas Espinoza[1], Mark McClure[2], Marcelo Pellicer[3], Iñaki Barrangu[3], Sebastian Olmos[4], Raul Varela[4], 1. The University of Texas at Austin, 2. ResFrac Corporation, 3. Pan American Energy, 4. Tecpetrol SA.

Abstract

Aggressive drawdown on unconventional wells commonly leads to the return of proppant pumped during the stimulation treatment, reducing propped fracture aperture, with potential impact on hydrocarbon production. Despite being identified by the available literature as a source of concern to operators, how much proppant flowback affects unconventional well production is a question that remains unanswered. This study quantifies the impact of proppant flowback on gas production under different drawdown scenarios through numerical simulations history-matched with proppant production measurements in the field.

The numerical simulations were performed with a fully coupled reservoir, fracturing and geomechanics commercial simulator (ResFrac) using its module to simulate proppant flowback. The physical model employed to quantify proppant production was tested, validated, and improved with this study. Two different operators shared proppant flowback and production data from two gas wells in the Vaca Muerta Formation (Argentina) to carry out this analysis. Such field data was utilized to history-match proppant flowback data from unconventional wells for the first time. The calibrated models were used to understand the effect of drawdown management on proppant flowback and its impact on early-time gas production and its estimated ultimate recovery. A series of sensitivity analyses on critical variables in the model were also conducted to further study the potential influence of proppant flowback on gas production under different conditions. Results show that proppant flowback may not always be detrimental to gas production, and that its influence varies depending on each case.

Introduction

During completion operations in unconventional wells, proppant agents are pumped to prop fractures open after pumping stops. Often, a portion of the proppant flows back into the wellbore with the produced fluid

during the clean-up phase after the stimulation. This phenomenon is known as proppant flowback and is highly undesirable since it can damage surface and downhole equipment (e.g., erosion of pipes, orifice, pumps, ESP, etc.) and may reduce well productivity.

Proppant flowback has been extensively studied in the laboratory. Parker et al. (1999) carried out a series of laboratory experiments performed with slot models (i.e., parallel plate device) and API linear conductivity cells to study the impact of key factors on proppant flowback. Their observations indicated that the critical fluid velocity required for proppant production increased with proppant size and decreased with closure stress. Goel and Shah (1999) presented results from tests conducted in a high-pressure slot model (tested up to 1000 psi in closure stress) and arrived at the same conclusions. They identified fluid flow rate, particle size, fracture width and closure stress as the critical variables that impact proppant production. Zhang and Guo (2016) conducted laboratory experiments to study critical flow velocity to trigger proppant flowback. They used a Barnett rock sample that was cut in half and had proppant placed between both pieces to simulate a propped fracture. Contrary to some previous studies, they observed that critical flow velocity increased with closure stress. The authors claimed that differences with previous observations are linked to the magnitude of the friction coefficient in the proppant grains. High closure stress increases normal forces pushing proppant grains outwards, but it also increases the friction force acting on the proppant. Thus, weak frictional forces taking place at the laboratory scale in previous studies due to low friction coefficients could explain previous observations. This is consistent with results presented by Guo and Wang (2022). They simulated proppant flowback in the laboratory by slot models with parallel steel plates and rock plates. Their observations also indicated that proppant production decreased with increasing closure stress at constant flow rates, and hence, at the field scale with larger flow rates, closure stress is expected to have an inhibition effect on proppant flowback.

Fundamental physical mechanisms of proppant flowback have been investigated before. Asgian et al. (1995) used a discrete-element numerical model to simulate the triggering of proppant flowback based on different combinations of parameters, including fracture width, proppant grain size and pressure drawdown. The study concludes that proppant packs are inherently unstable at ratios of aperture to proppant diameter greater than 5.5. Canon et al. (2003) further postulated that the main factors that determine proppant flowback are width ratio (i.e., ratio of fracture width to mean proppant diameter), closure stress, drag forces and proppant additives. This work concluded that width ratios wider than 6 are certain to cause fracture instability. Closure stress is also a key variable to consider. This study aligns with the idea that higher closure stress increases friction forces among grains and reduce probability of having an unstable pack. However, excessive closure stress that exceeds the nominal strength of the proppant can be responsible for proppant crushing and lead to flowback of proppant fines. These conclusions are in good agreement with the work by Shor et al. (2014). The authors introduced a discrete element model to model proppant dynamics during flowback that accounted for physical interaction between elements and tracked the mass movement of each element as collisions occur. Their simulations showed a clear dependence of proppant flowback on fracture width, confining stress, pressure gradient and proppant cohesion.

Recent studies have addressed the development of numerical models to capture proppant flowback integrated with hydrocarbon production at the field scale. Chuprakov et al. (2020) presented a model to predict and quantify proppant flowback. The equations to quantify proppant flowback in the model were tuned with laboratory observations. Their workflow comprised modeling a hydraulic fracture geometry with a numerical simulator, and posteriorly exporting results into their proppant flowback simulator. The authors tested the model with field observations from vertically fractured conventional wells by matching one cumulative proppant mass data point after a few months and not a continuous curve of proppant mass rate. They ran a sensitivity on fracture design and their results showed that one of the simulated cases with proppant flowback outperformed a different case without proppant production. This is consistent with proppant mass cumulative values that they presented from 4 different wells compared to oil production, where no clear trend could be observed between well performance and proppant production. Recently, Pandey (2023) developed a numerical simulation model to predict the occurrence of proppant flowback

based on comparing estimated flow velocities at the cluster stage with predicted critical velocities to trigger proppant production in three wells. The study shows that only a portion of clusters in a fracture stage produced proppant in the model.

Since proppant flowback sensitively depends on pressure gradient, then the wellbore drawdown management strategy plays a key role in mitigating proppant flowback. Karantinos et al. (2015) claims that proppant flowback can be reduced or avoided by the selection of an optimum production strategy. However, operators are usually inclined to employ aggressive drawdown strategies in wells to accelerate production and reduce clean-up times. This causes proppant pack instability that increases likelihood of proppant flowback occurrence. While the latter is normally presented as a concern to hydrocarbon production in unconventional wells, no previous published work has quantified production losses in the field due to proppant flowback via numerical simulation. Without such analysis, it becomes hard for an operator to assess the risks associated with proppant flowback, if any, and to react accordingly.

The objective of this study is to introduce a workflow to model and forecast proppant production using a fully coupled reservoir, stimulation and geomechanics commercial simulator. First, we incorporate a set of equations into the model to predict proppant flowback occurrence and quantify its production. Then, we test and calibrate the model using field data of unconventional wells shared by two different operators. Finally, we quantify the impact of proppant flowback on gas production under different drawdown managements and conditions. This study and analysis can also be useful to operators to forecast proppant production, estimate harm to pipelines and downhole equipment by proppant erosion, and design desanders accordingly.

Semi-Mechanistic Model to Predict Proppant Flowback Occurrence

The set of equations utilized in this study to predict the triggering of proppant flowback are based on the semi-mechanistic model proposed by Canon et al. (2003) derived considering the following statements:

- The interaction between net closure stress, drag force and fracture width can be used to define regions of proppant stability. Wide fractures will almost always tend to be unstable.
- There is a minimum fluid velocity necessary to drag proppant grains in every case.
- The strength of the proppant material contributes to define a mechanical destabilization region (e.g., proppant crushing)

The stability criterion in the model is defined as:

$$F_{STA} = 1422.5 \exp(-1.0483\, W_r) \exp\left[-0.5\left(\frac{ln(P_{c,net})-a'}{3x10^{-5}\, S_{MAX}+0.22368}\right)^2\right] + 1.365x10^7\ \frac{v_f\, \mu_f}{k_f} \qquad \text{(Eq.1)}$$

Where $P_{c,net}$ is the net closure stress, S_{MAX} as the nominal strength of the proppant, μ_f is fluid viscosity, k_f is proppant pack permeability, v_f is the critical velocity for loose proppant grains mobilization (Eq. 2.3), a' is a constant equal to 7.7172, and W_R is the ratio of fracture width and average proppant diameter (known as width ratio). The minimum critical velocity for loose grains mobilization comes from Ergun's equation (Canon et al., 2003), and depends on fluid viscosity, the specific gravity of the proppant, fluid density, proppant grain diameter and the minimum porosity for fluidization. In the numerical simulator, this porosity is inputted as the porosity of the proppant pack in each fracture element. The outcome of this model is the stability threshold for the pressure gradient acting on the proppant pack, called F_{STA} in the cited work.

Proppant Flowback Modeling in ResFrac

The simulations in this study were carried out in ResFrac, a commercial fully coupled reservoir, fracturing and geomechanics numerical simulator. The model employs the finite volume method and solves a set of

equations at every time step for each block. These include molar mass balance, proppant mass balance, energy balance and water solute mass balance (McClure et al., 2022). Ultimately these equations are solved to calculate fluid (and proppant) transport throughout the mesh over time.

The set of equations to predict the triggering of proppant flowback in the numerical model are based on the semi-mechanistic model by Canon et al. (2003). The outcome of the semi-mechanistic model is the stability threshold for the pressure gradient acting on the proppant pack (F_{STA}) mentioned above. This value is calculated in each block along the fracture mesh at every time step and is compared to the pressure gradient acting on the proppant pack. If the pressure gradient is greater than the limit, proppant is allowed to flow. Physical aspects not fully captured by the semi-mechanistic model, like fracture roughness, proppant shape (e.g., rounded versus sharp-edged), proppant type (e.g., resin-coated or ceramic), etc. could deviate the model predictions from field observations. For this reason, a tuning parameter A is added at the end of Eq. 1:

$$F_{STA_{model}} = F_{STA} + A \quad \text{(Eq. 2)}$$

It should be noted that the semi-mechanistic model presented by Canon et al (2003) was derived solely to predict proppant pack instability and does not quantify proppant mass production. For this reason, we formulated an equation to calculate proppant mass rates in the model every time the threshold gradient is surpassed:

$$\dot{m}_{FBK} = \dot{m}_{prop} * \chi \quad \text{(Eq. 3)}$$

$$\chi = 1 - \frac{1}{1+m\,\Delta P_{rel}{}^{n}} \quad \text{(Eq. 4)}$$

$$\Delta P_{rel} = \frac{\Delta P_{grad} - F_{STA}}{F_{STA}} \quad \text{(Eq. 5)}$$

Eq. 3 to 5 quantify proppant mass rates in the model. This is the result from the product of mass flow rate calculated in the simulator with the transport equations during injection times a multiplier. The simulator calculates proppant transport during injection accounting for proppant bridging, viscous drag and gravitational settling rate of each proppant type (McClure et al., 2022). Proppant mass rates are expected to be lower during proppant flowback due to the compressive stress of the fracture walls acting on the proppant pack. Thus, the χ-multiplier in Eq. 3 should be lower than 1. This is calculated by Eq. 4 via an empirical sigmoidal relationship with the relative difference between the threshold gradient for proppant pack instability (F_{STA}) and the pressure gradient acting on the proppant pack (ΔP_{grad}). This function shape is based on the notion that greater differences between the gradient and the estimated limit should lead to greater proppant instability and, therefore, greater proppant mass rates. In Eq. 4, the m-parameter, or proppant slip factor, controls the rate at which proppant mass is allowed to flow out of the pack at a given pressure gradient excess. This proppant slip factor should be physically associated with fracture roughness, proppant type and shape (e.g., resin-coated proppant could have lower m values), proppant pack distribution and restrictions in the proppant flow path. The n-exponent impacts the shape of the sigmoidal curve. Higher exponents lead to lower rates at low gradient pressure differences with respect to F_{STA}, and higher rates when there is greater difference between gradients. In the simulated wells, the model best replicated field data with $n = 1$.

Model Set-Up and History-Matching Considerations

Building the numerical model involves the definition of an appropriate mesh size, reservoir fluid PVT properties, reservoir fluid saturation, rock properties, formation pressure gradient, proppant size and

additional relevant properties. The two operators that supported this study shared their estimated petrophysical properties, subsurface stress interpretations, completion reports and production data to model each case. All imported data is associated with multi-stage hydraulically fractured horizontal gas wells.

The model is used to simulate both the stimulation treatment and the production stage of the wells. The goal behind building the model is to replicate proppant flowback production measured in the field. As elaborated above, proppant flowback strongly depends on the pressure gradient exerted on the proppant pack. Proper modeling of proppant flowback therefore requires high level of mesh refinement, especially close to the well, where the pressure gradient along the fracture is highest. Thus, we decided to model only one fracture stage to decrease computational demand as much as possible without losing physical representativity. Modeling a scale lower than a complete fracture stage (e.g., single fracture) would complicate production allocation and would bring a higher degree of uncertainty into the study. Modeling an entire fracture stage allows to capture stress shadow effects between fractures, and accounts for differences in pressure drop and proppant transport between perforations. These can result in different fracture geometries between clusters that can impact proppant flowback behavior. Raterman et al. (2019) showed that some stages may contribute more fluid than others, and that the production distribution is not always uniform in the well. However, in wells with multiple fracture stages with no obvious geological differences across the lateral, even if some stages deviate from the average, the linear upscaling of a single fracture stage should still provide a representative model of the average behavior of the well.

The discretization of the pressure gradient simulated close to the wellbore depends on the element dimensions in the near wellbore region. Hence, proppant flowback modeling can be mesh size dependent. We carried out a sensitivity analysis on fracture grid block dimensions to select the most appropriate mesh size, under the premise that more refined grids lead to more accurate results. As a result, fracture element dimensions were set to be 25ft laterally and 12.5ft vertically.

The reservoir matrix grid was first subdivided into vertical layers using the operator's interpreted minimum horizontal stress logs (Figure 1). The model discretizes interpreted stress logs to capture high-contrast stress zones that may act either as fracture growth preferential zones or as fracture barriers. Once defined, each layer is assigned stress, porosity, rock elastic properties and fluid saturation inputs after proper average of the log values within those sections. Initial rock permeability and relative permeability curves remain constant through the entire grid in the model initialization. We considered slight anisotropy in the permeability by specifying vertical permeability as one tenth of the horizontal permeability. The reservoir pore pressure gradient in the modeled formation is approximately 0.8 psi/ft. Thus, the reservoir is strongly over-pressured, which supports the addition of stress-dependent decay in matrix permeability to account for pore throat shrinkage with depletion (Heller et al., 2014). This is modeled as an exponential relationship of permeability against effective stress defined by its decay rate (rock gamma).

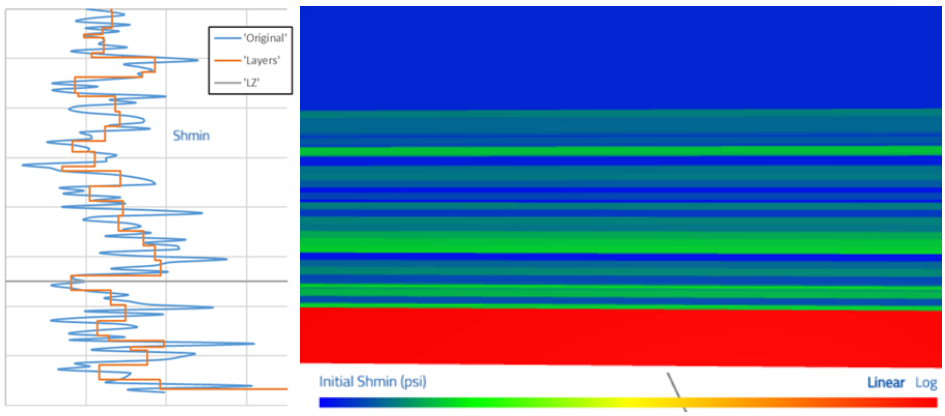

Figure 1: Minimum stress log with associated discretized layers (left); and layer definition in the model based on minimum stress values (right).

Proppant properties are critical to the simulation. The model uses the modified Carmen-Kozeny equation (Krauss and Mays, 2014) to calculate proppant pack permeability, and thus, propped fracture conductivity:

$$k_{f_{c,prop}} = k_{0,b} \frac{d^2(\phi - f_b)^3}{(1-\phi+f_b)^2} \quad \text{(Eq. 6)}$$

Where d is proppant diameter, ϕ is proppant pack porosity, and $k_{0,b}$ and f_b are calibration parameters. The value for f_b is generally defined as zero to simplify tuning the model with only the value of k_0. The latter is tuned with production data. Inputting a low number can result in finite dimensionless fracture conductivity that can prevent fitting the model to field production data during the first months of production. The proppant pack permeability loss with depletion is modeled as an exponential decay against effective stress acting on the grains and is defined in the model by its exponential decay rate (fracture conductivity gamma). This value is set as $2 \cdot 10^{-4}$ psi^{-1} and is tested in a sensitivity analysis carried out at the end of this study.

We normalized gas, water, and proppant mass production curves to a single fracture stage by dividing total well production by total number of stages. The model uses the bottom-hole pressure (BHP) curve as the input boundary condition to simulate production rates. The BHP curve describes the drawdown management followed by the operator and, thus, determines the pressure gradient exerted on the proppant pack during production. It is common practice to record surface pressure in gas wells by operators in the Vaca Muerta Fm. This is converted from wellhead to bottom-hole pressure through the 'Gray' correlation (Gray, 1978).

The model was then calibrated to replicate field observations including instantaneous shut-in pressure (ISIP) at the end of the modeled fracture stage, fluid production rates and cumulative curves, proppant mass production cumulative, and additional observations shared by the operator that helped to narrow down fracture geometry (e.g., non-communication between benches seen with tracer tests, pressure interference tests, well spacing description, etc.). We varied the fracture toughness in the model and its relative increase with the square root of fracture height or length (whichever is smaller) to limit fracture size and to approximate the estimated ISIP (McClure et al., 2020; 2022). ISIP is also influenced by complex near wellbore effects that are hard to capture (McClure et al., 2023), thus ISIP in the model was approximated to the interpreted ISIP from the fracture report without attempting a perfect match. Fracture toughness and its relative increase in the model also affect fracture aperture, which has a strong impact on proppant pack instability. Therefore, this was used together with parameters in Eq. 3 and 5 to also calibrate proppant mass production to field observations. Rock permeability, relative permeability curves, stress-dependent rock permeability decay rate, and initial proppant pack permeability were also tuned in the model to reproduce field production data.

Proppant mass production can be further adjusted by a set of three parameters: m, n and A from Eq. 2 and Eq. 4. Parameters m and n affect the rate at which the model proppant mass flows back from the fractures into the well. Increasing values of m imply that proppant flow will reach higher initial rates and will flow faster from the fracture (Figure 2). Reasonable values for the proppant slip factor are within 10^{-4} and 10^{-2} based on the model results. The n-parameter modifies the shape of the sigmoid curve. A value of 1 best replicates field observations in the modeled wells. It should be noted that while m can impact the total mass production cumulative in the long term, the maximum proppant mass that can be produced is mostly defined by the semi-mechanistic model. Thus, fluid rheology, fluid velocity, net closure stress, initial proppant concentration and specially fracture width ratio are the main variables that determine the upper limit of this outcome in the model.

Parameter A shifts the threshold pressure gradient for proppant pack instability obtained using the semi-mechanistic model by Canon et al. (2003). Positive A values involve delaying the start of proppant production, while negative values bring it forward in time (Figure 2). Because this parameter modifies the limit for proppant stability throughout the entire simulation, it will also moderately impact proppant mass

cumulative between cases. Ideally, this value should be close to zero to prevent large deviations from the correlation by Canon et al. (2003).

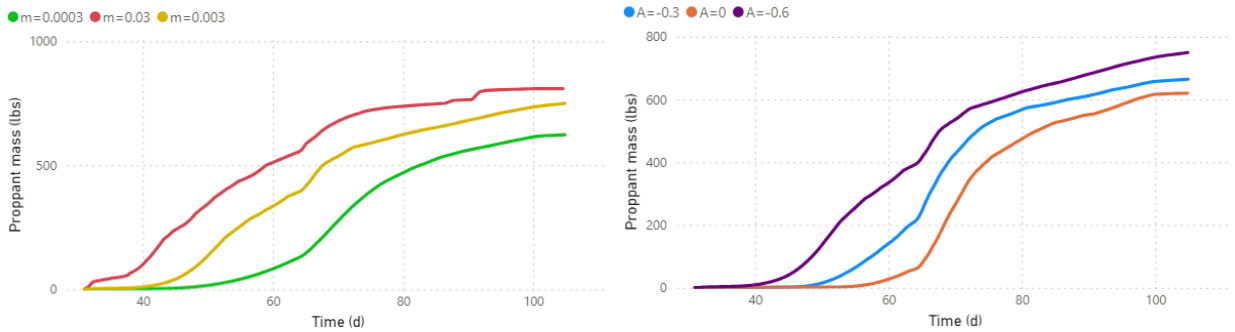

Figure 2: Sensitivity of proppant mass production to *m*-parameter (left) and to *A*-parameter (right).

Case Study of two gas wells in Vaca Muerta

We ran the workflow for two multi-fractured horizontal gas wells from different fields in Vaca Muerta Fm. shared by two different operators. The Vaca Muerta Formation is currently the main unconventional target in Argentina. This source rock is situated in the Neuquen Basin, in West-Central Argentina with over 1000 unconventional wells drilled and stimulated so far (Figure 3). Vaca Muerta ranks second worldwide in shale gas resources and fourth in shale oil resources (EIA, 2013).

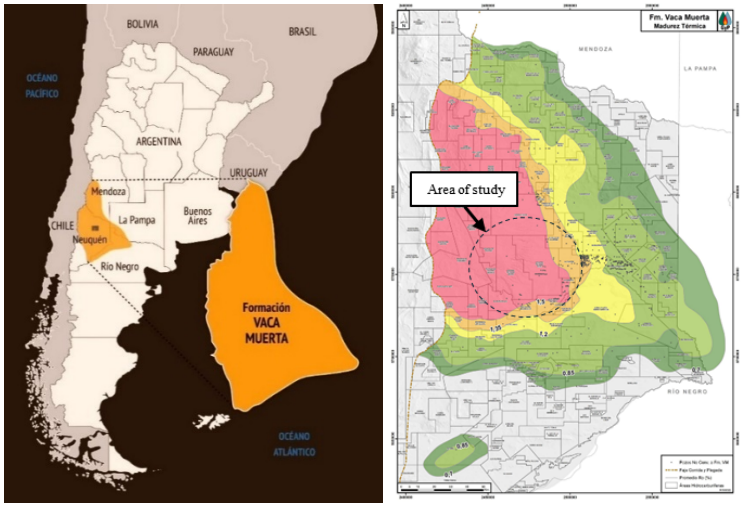

Figure 3: Geographical location (left) and thermal maturity map (right) of Vaca Muerta Fm. based on vitrinite reflectance, indicating lease borders and fluid windows (modified from https://www.argentina.gob.ar/economia/energia/vaca-muerta/mapas & https://www.energianeuquen.gob.ar/vaca-muerta-madurez/).

The completion design was similar in the two modeled wells. Both wells were completed with multi-clustered plug-and-perf operations. Slickwater and high-viscosity friction reducer (HVFR) were utilized as fracturing fluids during the stimulation treatment of the two wells. Proppant agents of mesh 100 were initially pumped, followed by larger-sized proppant grains during the second half of the treatment.

Proppant mass production is generally only measured during the initial testing stage of the well, in which individual fluid separators and desanders are available for each well in the pad. This period usually lasts about three months. After that, depending on the operator's practices, the desander is either removed from the well or left installed but with no consistent proppant mass measurements during its discharge. For this reason, while gas production in each case was calibrated with a whole year of historical measurements, simulated proppant flowback was only calibrated using the first three months of proppant production.

However, this is the period in which operators open the choke size until the well reaches its peak production rate, thus it is the time in which proppant production is highest. Therefore, it is enough to obtain a well-calibrated model on proppant flowback behavior.

Well 1: High Proppant Production

We calibrated a model that reproduces all the key field observations to an acceptable degree. The input BHP curve was smoothed to reduce noise and instabilities in the model. Figure 4 compares the field drawdown curve with the smoothed curve prescribed in the model, together with the production curves from the model measured in the field. There is a very good match in gas production, not only in the cumulative curve but also in the daily gas rates, which are key to predict the proppant pack stability. There is a minor difference in water cumulative which does not impact proppant flowback results in the simulation.

The model accomplished a remarkable match of proppant mass production. Figure 5 compares mass production rates and proppant mass cumulative curves between the model and field measurements. Even the continuous peaks and troughs in proppant rates through choke size ramp-up during the first two months of production were replicated accurately. Such close matching gives confidence in the results of the model concerning the sensitivity analysis to drawdown. The model also captures proppant mass production from the two different mesh sizes injected during stimulation. The results are consistent with field observations reported by the operator, which report more than one proppant size retrieved in the well when discharging the desander box.

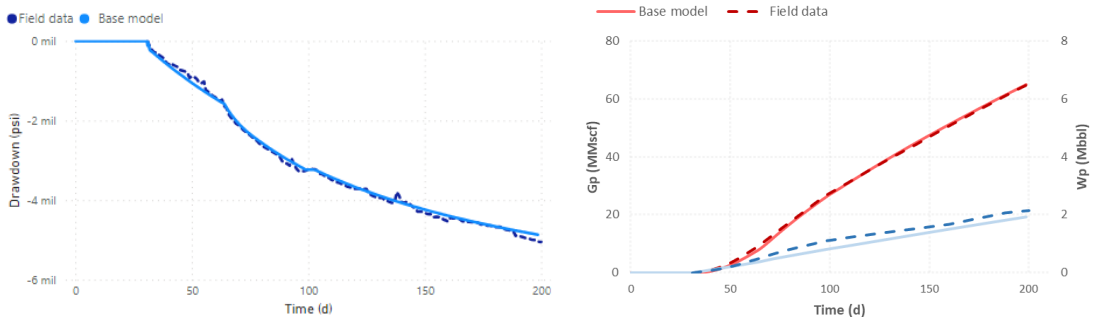

Figure 4: Field versus simulated drawdown for *Well 1* (left); field versus simulated water (blue curve) and gas cumulative production (red curve) for *Well 1* (right).

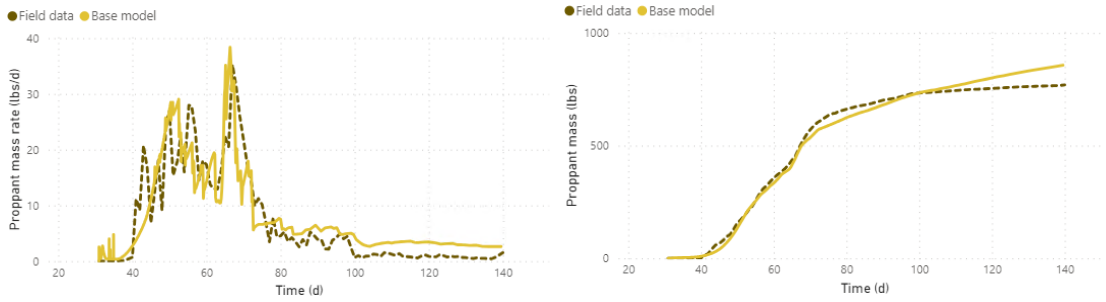

Figure 5: Field versus simulated proppant mass production rates (left) and proppant mass production cumulative (right) for *Well 1*.

Figure 6 shows the differences in proppant mass, gas and water production between fractures created in each cluster, compared to the initial near-wellbore-region width ratio (ratio between fracture width and average proppant diameter). There is a strong correlation between proppant production and width ratio, which was expected considering its influence on the proppant pack stability determination. Additionally, proppant mass production is scattered and does not seem to be associated with gas production. Clusters with similar hydrocarbon production show completely different results of proppant flowback. That means that even if a well experiences proppant flowback, this phenomenon does not necessarily harm the most

productive fractures. For instance, fractures from clusters 6 and 7 show the greatest gas production and produce less proppant than most other clusters. This behavior can be explained by the fact that gas production depends mostly on fracture area (Wattenbarger et al., 1998), while proppant mass production is mostly dependent on fracture aperture. This non-uniformity in proppant production allocation between clusters is consistent with simulation results presented by Pandey (2023). Fractures originated in some clusters develop greater width ratios that are more unstable, and thus flow more proppant mass back into the well. Even in the case that proppant flowback decreases fracture hydrocarbon productivity to some degree, it would only be affecting a portion of the total fractures contributing to total production.

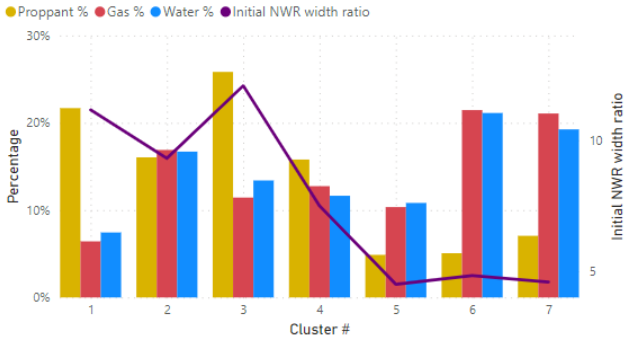

Figure 6: Relative contribution of each cluster to the total simulated proppant, gas and water production cumulatives after 10 years of production (bars); and simulated initial width ratio close to the wellbore per cluster (line).

We then carried out a sensitivity analysis on drawdown management. We defined four drawdown strategies in addition to the base case (*Moderate DD*): conservative, medium, aggressive, and extreme. Figures 7 and 8 show the differences in gas, water, and proppant mass production at these different drawdown strategies. Gas cumulative production was normalized by the cumulative production in the base case after 10 years of production to ease comparison between cases. As expected, the well flows back more proppant with more aggressive drawdown strategies. Proppant drainage radius around the well increased from an initial 12.5ft to 50 ft in most clusters in the *Extreme DD* case, which explains the large increase in proppant flowback. This is also reflected in more uniform proppant cumulative between clusters compared to the base case, with each cluster contributing 10-20% of total proppant mass recovered. Proppant production after 10 years increased from 0.8% of the injected mass in the base case to 4% in the extreme case. Even at this extreme drawdown, the fracture remained propped adjacent to the well as fracture width ratio near the wellbore decreased to a final value of 2, after which the proppant pack remained stable through the rest of the simulation (Figure 9).

Despite the clear spike in proppant production, there is no significant difference in the 10-year gas cumulative production between cases (Figure 7). We re-ran all cases without allowing proppant to flow back (this can be achieved by setting *m*-parameter equal to zero in the model in Eq. 5) to better understand the impact of proppant flowback in the model. Results indicated that in this set of scenarios, proppant flowback does not affect gas production. This occurs because even though fracture conductivity near the wellbore decreases up to 7 times as a result from fracture width reduction at greater proppant flowback, it does not drop enough to significantly alter the total effective fracture conductivity (Figure 9). Figure 10 shows that the pressure gradient in the fractures in scenarios with and without proppant production remains low and almost the same even in the *Extreme DD* case. This is further reflected by *FCD* values not falling below 100 in any case, which is the threshold commonly defined to separate finite from 'infinite' fracture flow capacity (Agarwal et al., 1979; comments on *FCD* estimation are provided in the Appendix). *FCD* derivation intrinsically assumes boundary-dominated radial flow (Cinco-Ley et al, 1978), therefore it is not perfectly representative for linear flow in a shale (Almasoodi et al, 2023), but it is still presented to provide a simple and widely used reference.

Thus, production remains unaltered despite the drop in fracture flow capacity near the wellbore. This is consistent with observations provided by the operator, reporting no changes in well productivity and long-

term gas cumulative between wells subjected to more aggressive drawdown management in the field, despite recovering more proppant. The operator, however, did not try drawdown strategies beyond the medium case.

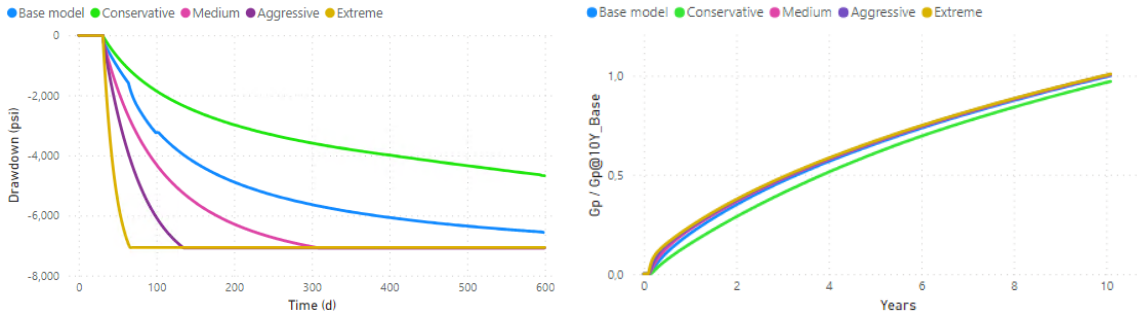

Figure 7: Drawdown management and gas cumulative by case in the *DD* sensibility analysis for *Well 1*.

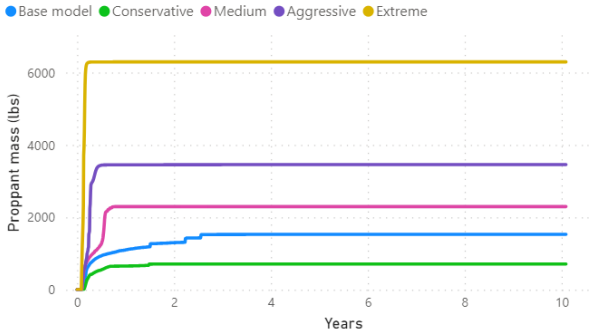

Figure 8: Proppant mass production cumulative by drawdown case for *Well 1*.

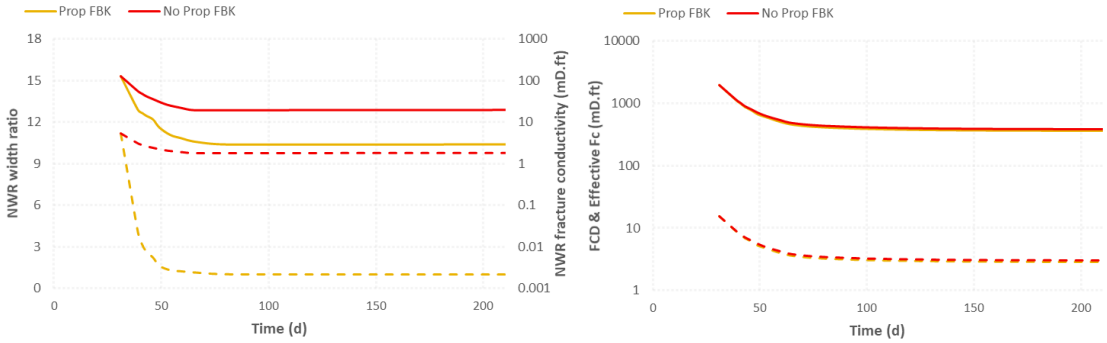

Figure 9: On the left, simulated width ratio near the wellbore (dashed lines) and the associated near wellbore fracture conductivity (full lines) against time in cluster 1 (contributed 20% of well proppant production) in the *Extreme DD* case with and without (red) proppant flowback; on the right, simulated effective *Fc* (dashed lines) and *FCD* (full lines) in cluster 1 in the *Extreme DD* case with (yellow) and without (red) proppant flowback. In early stages, fracture conductivity decreases due to the stress effects on proppant pack permeability.

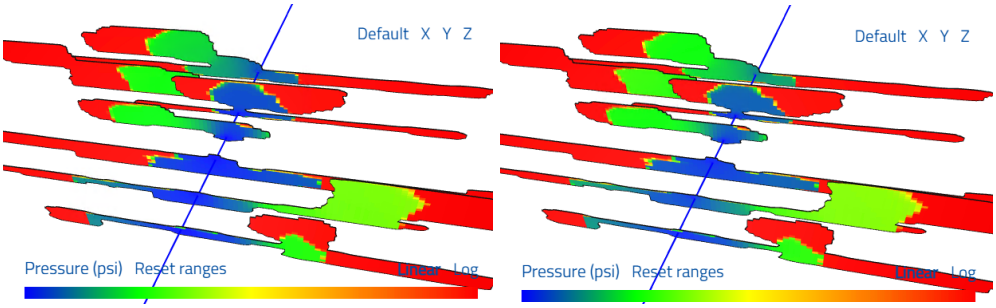

Figure 10: Pressure gradient along the fracture after 6 months of production in the *Extreme DD* case with (right) and without (left) proppant flowback for *Well 1*. There is negligible variation in the pressure gradient between cases.

Well 2: Low Proppant Production

Well 2 is based on another gas well in production from the Vaca Muerta Fm in a different field and operated under different conditions than *Well 1*. Well spacing in this pad is substantially wider than in the previous case. Similar to *Well 1*, the model of *Well 2* was history-matched to reproduce field observations. The model results align very well with field gas and water production rates and cumulative values (Figure 11). Drawdown management, used as input in the model, is more conservative than in *Well 1*, which partially explains why proppant production is also considerably smaller (Figure 12). The model was calibrated with a 20-times lower proppant slip factor or *m*-parameter compared to *Well 1*. This could be associated with differences in the stress states and geologic complexities impacting fracture growth, different completion designs (e.g., *Well 2* has larger number of clusters and number of perforations per cluster and had a bigger proppant grain size pumped at the end of treatment), and with the wider well spacing leading to weaker stress shadow effects between wells, which would pose fewer restrictions to fracture growth and could have led to more stable proppant packs. Furthermore, the initial fracture width ratio close to the well is narrower in most fractures in *Well 2* than in *Well 1*.

The proppant drainage radius for this case is 12.5ft, comparable to *Well 1*, but the quantity of drained mass is considerably smaller. Proppant production is not uniform between clusters and is not localized in the best producing clusters only. The simulation indicates a strong correlation between initial width ratio near wellbore and proppant production in each cluster (Figure 15).

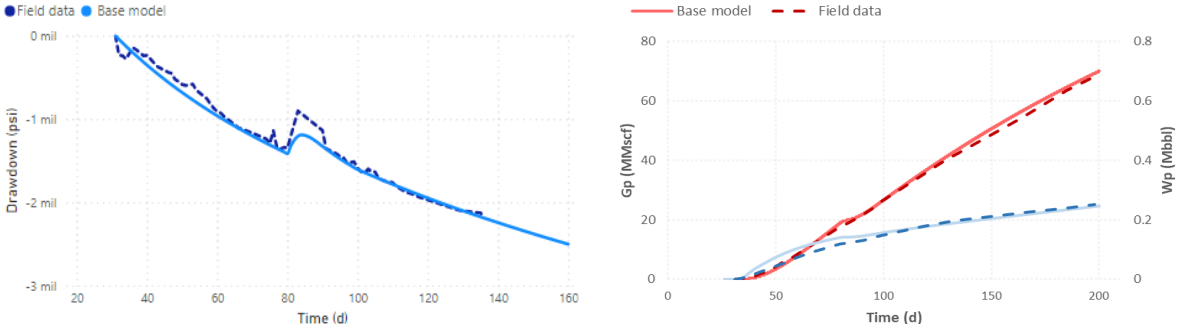

Figure 11: Field versus simulated drawdown for *Well 2* (left); water (blue curve) and gas cumulative production (red curve) for *Well 2* (right).

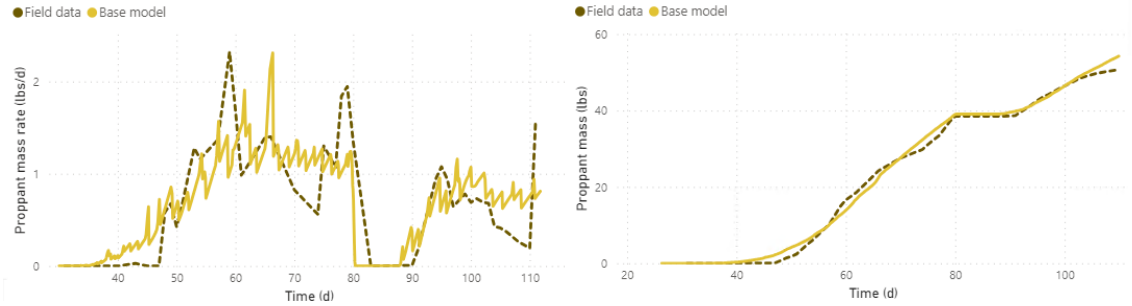

Figure 12: Field versus simulated proppant mass production rates (left) and cumulative (right) for *Well 2*.

Same as in *Well 1*, we ran the model with a series of different drawdown strategies to study the variation in proppant production and evaluate its impact on gas recovery. Figure 13 presents the set of drawdown curves applied in the model. The base case corresponds to a conservative scenario in this comparison set. Gas cumulative production after 10 years is similar between cases (Figure 13). Final proppant mass cumulative grows with more aggressive drawdowns, and peaks at almost 600 lbs in the *Extreme DD* case (Figure 14). This mass represents only 0.4% of the injected proppant, 10 times lower than *Well 1* under the same drawdown management. The results indicate a more stable proppant pack in *Well 2* than *Well 1*.

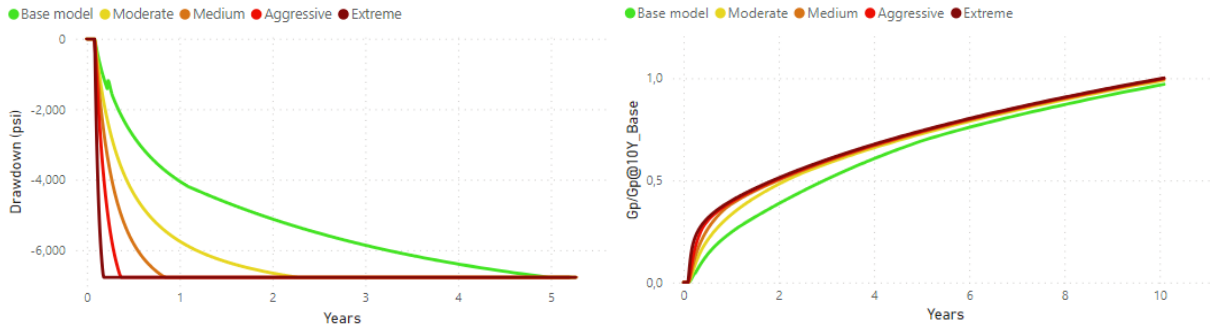

Figure 13: Drawdown (left) and normalized gas cumulative (right) by case in the *Fc* sensibility analysis for *Well 2*.

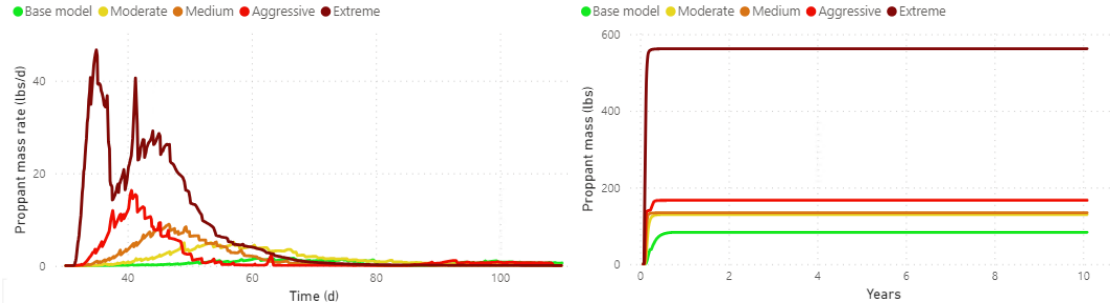

Figure 14: Proppant mass production rates (left) and cumulative (right) by drawdown case for *Well 2*.

Proppant drainage radius in the *Extreme DD* case reaches 25 ft in cluster 1, which contributes the most proppant mass. This drainage is much lower than what was observed in *Well 1*. Fracture width ratio and conductivity near wellbore are reduced 3-times from their original values in this cluster. However, the effective fracture conductivity and *FCD* do not significantly change and stay above 100. Figure 15 shows that proppant production becomes more uniform between clusters under a more aggressive drawdown, similar to the observations in *Well 1*. The most affected clusters lose less than 2% of gas production, while half of the clusters do not suffer gas production losses at all. When comparing cases with and without proppant flowback, the overall gas production loss due to proppant flowback in the *Extreme DD* case is less than 1%.

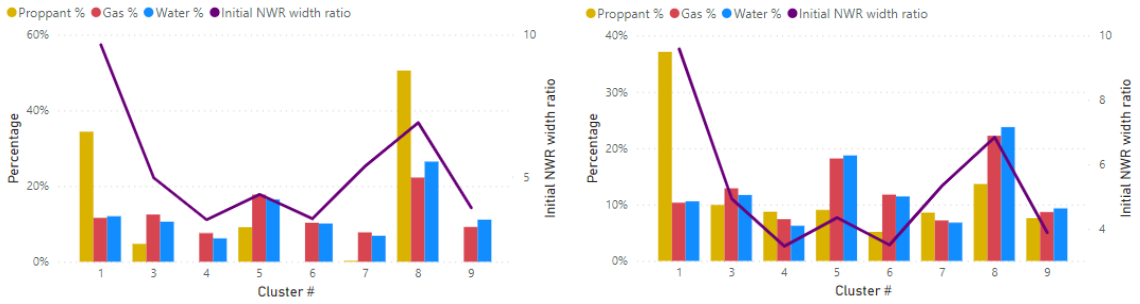

Figure 15: Relative contribution of each cluster to the total simulated proppant, gas and water production cumulatives after 10 years of production (bars) and initial width ratio close to the wellbore per cluster (line) in the *Base model* (left) and in the *Extreme DD* case (right).

Sensitivity Analyses

The previous results suggest that proppant flowback might not significantly impact production in cases with large initial fracture conductivity (i.e., 'infinite' fracture flow capacity), absence of time-dependent (not the same as stress-dependent) fracture conductivity damage and moderate proppant pack permeability compressibility. In this section, we explore the differences in results by varying these parameters in the model.

We carried out a series of sensitivity analyses to understand the impact of proppant flowback on gas production under more adverse conditions. We ran the new simulations for *Well 1* due to its greater proppant production, more prone to impact gas production than *Well 2*. We tested cases with lower initial fracture conductivity, higher stress-dependent proppant pack permeability decay rate, absence of stress dependence of rock permeability, and time-dependent fracture conductivity. It should be noted that some of these cases produce lower gas rates, and thus display slower fluid velocities and lower proppant production (Figure 16). For this reason, we forced the new cases to have the same amount of proppant production as the base case simulations of *Well 1* at each corresponding drawdown. In this way, we can study the differences in gas production given the same amount of proppant flowback under more adverse conditions for the fracture flow capacity. There was no need to modify the modeled proppant flowback curve in the time-dependent conductivity sensitivity since the simulated proppant mass cumulative was almost identical to the base model.

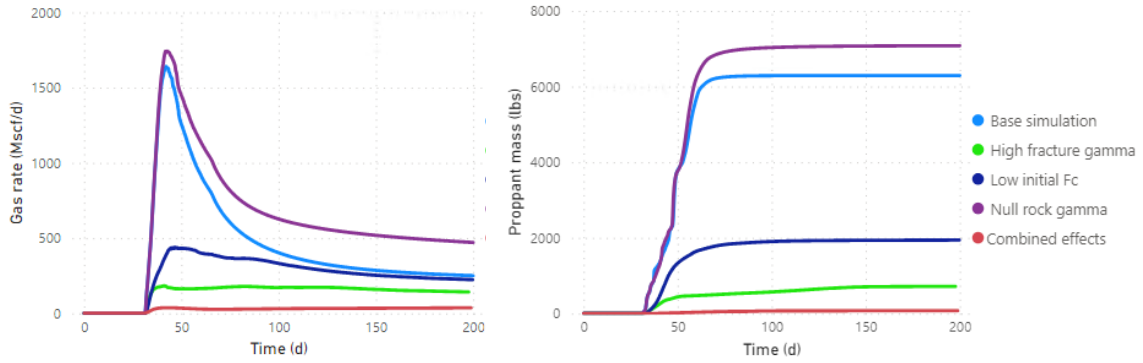

Figure 16: Gas rates of the *Extreme DD* case in the base model for *Well 1* and the new sensitivity cases (left); and proppant mass cumulative in the same new cases compared to the proppant cumulative in the base case simulation (right).

Sensitivity with lower initial fracture conductivity

The base model needed to be calibrated with a relatively high initial fracture conductivity, given by the initial aperture and the value of k_0 in the modified Kozeny-Carmen equation (Eq. 6). This resulted in an 'infinite' dimensionless fracture flow capacity throughout the entire simulation (i.e., low pressure gradient along the fracture). This is consistent with observations from RTA diagnostics and was necessary to obtain a match in early-time production (Figure 17). However, this might not apply to every case. Previous works have reported bigger fracture pressure gradients seen in wells in Bakken and the Midland Basin estimated from pressure measurements close to the fractures at varying distances in slanted monitor wells (Liang et al., 2022, Benish et al., 2024). Thus, we run a case with lower initial fracture conductivity by shrinking k_0 ten times in Eq. 6 to study the impact of proppant flowback on gas production when exposed to larger pressure gradients in the fracture.

Figure 18 shows that the pressure gradient along the fracture in the case with lower k_0 is considerably greater than in the base case. This was observed in *FCD* values falling below 100 in most clusters after the initial months of production. This means that fracture flow capacity is no longer 'infinite' compared to the matrix and can now create an additional restriction to fluid production.

The current simulation was re-run without proppant flowback to understand its impact on gas production in this new scenario. Opposite to previous results, the reduction in fracture aperture near the wellbore and the greater pressure gradient along the fracture lead to a non-negligible decrease in the effective fracture conductivity and *FCD* after proppant flowback (Figure 19). There is a 10% loss in gas cumulative in the first year, and an overall 5% loss after 10 years of production (Figure 19). As expected, gas cumulative in both cases is reduced compared to the base case with higher k_0.

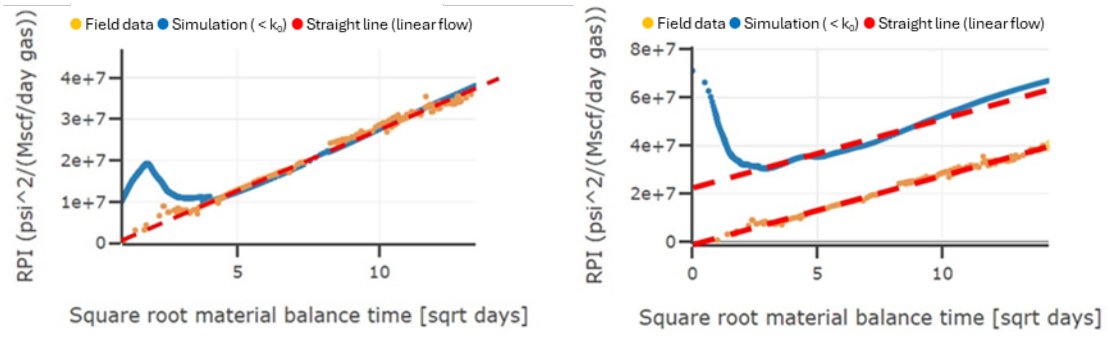

Figure 17: RTA plot with field data (orange curve) and results from the simulation (blue curve), comparing high (left) and low (right) k_0 values. An intercept higher than zero means there is an additional restriction to flow caused by 'finite' fracture conductivity.

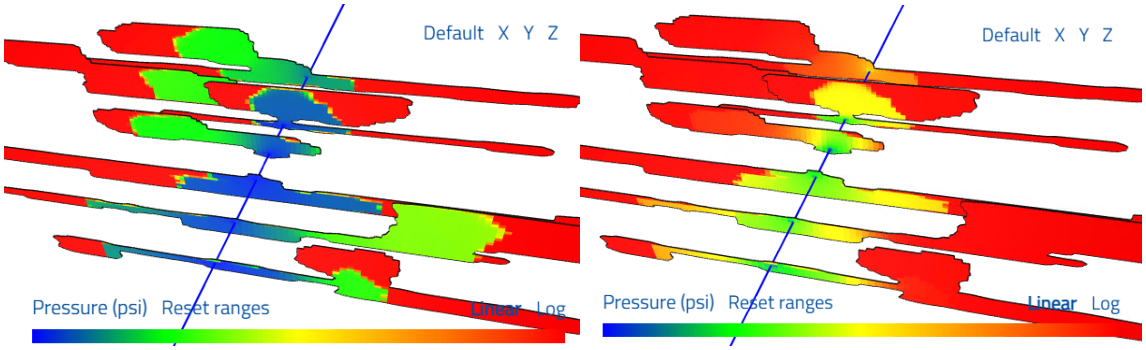

Figure 18: Pressure gradient along the fractures in the *Extreme DD* case with higher (left) and lower (right) initial fracture conductivity after six months of production.

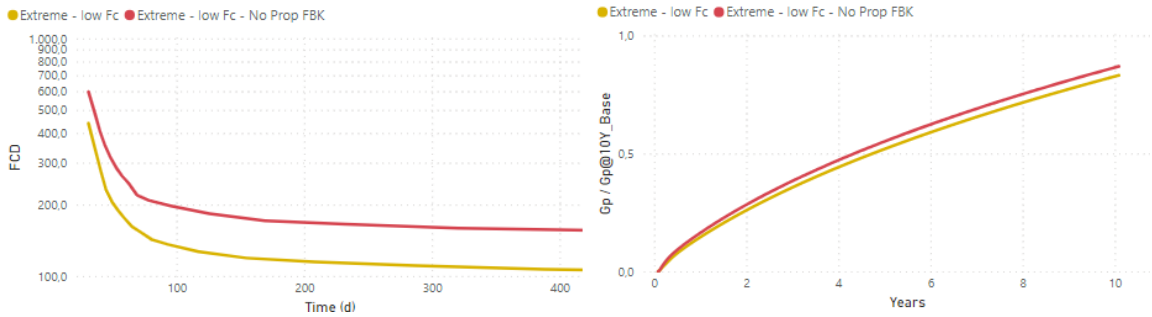

Figure 19: *FCD* curves for the *Extreme DD* case with low initial *Fc*, with (yellow curve) and without (red curve) proppant flowback (left); and gas cumulative in the *Extreme DD* case with low k_0 with (yellow curve) and without (red curve) proppant flowback (right).

Sensitivity with higher fracture permeability gamma

The decay rate of fracture conductivity with stress (i.e., fracture gamma) can lead to greater pressure gradients along the fracture as drawdown increases. Even if the dimensionless fracture conductivity behaves initially as 'infinite-acting', this condition could eventually cease, and wellbore productivity could deteriorate. Values of propped fracture conductivity gamma have been reported mostly in the order of 10^{-4} psi^{-1} and up to $1 \cdot 10^{-3} psi^{-1}$ in previous works (Ghassemi et al., 2012; McGinley et al., 2015). The current sensitivity analysis was carried out adopting this higher-end value to grasp a better sense of the impact of fracture conductivity gamma on proppant flowback and its effect on well productivity.

Same as in previous cases, simulations were run with and without proppant flowback. Because of the quick major reduction in fracture conductivity with stress, the pressure gradient in the fracture is greater than in previous cases at early times (Figure 20). Therefore, *FCD* rapidly falls below 100 in all clusters in the

simulation. There is a 10% loss in gas cumulative in the first year, and a 6% drop in the 10-year gas cumulative due to proppant flowback (Figure 20).

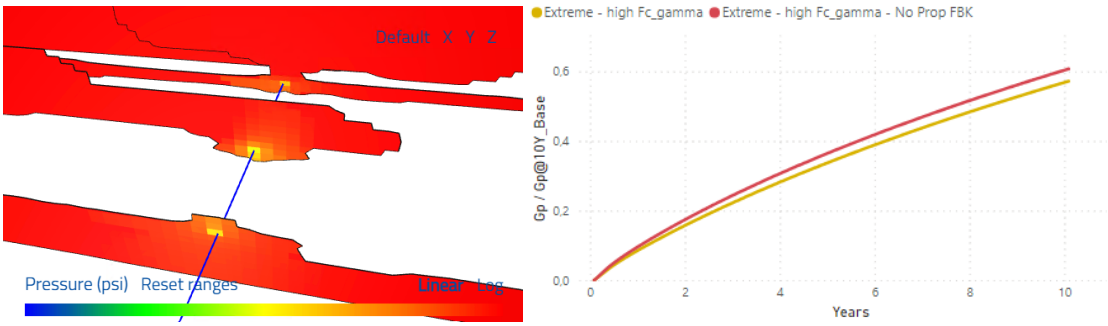

Figure 20: The pressure gradient along the fracture after 3 months of production in the *Extreme DD* case with high fracture permeability gamma (left); and the gas cumulative in this case with (yellow curve) and without (red curve) proppant flowback (right).

Sensitivity with null rock permeability gamma

Multiple works have studied the impact of net effective stress increase on shale permeability as the reservoir is depleted (Kwon et al., 2001; Heller et al., 2014). Declining rock permeability results in lower matrix flow capacity, which may choke the flow and impede the fracture from creating any restriction at all. The degree of pore throat narrowing and permeability reduction, however, may strongly vary between fields. For this reason, the current section shows results after running the model without rock dependent permeability to investigate how this affects the impact of proppant flowback on gas production.

Although the pressure gradient in the fracture is slightly greater in this case than in the base simulation with non-zero rock gamma, the effective fracture conductivity does not change significantly with proppant flowback and *FCD* remains above 100 in all clusters through the entire simulation. The drop in 10-year gas cumulative between cases without rock gamma, with and without proppant flowback, is only 2%.

Despite a greater matrix flow capacity with depletion compared to the reference case, the initial fracture conductivity is still too high for proppant flowback to cause a significant impact on gas production. For this reason, the model with null rock permeability gamma was run again reducing initial fracture conductivity ten times (i.e., k_0 divided by 10) to investigate if proppant flowback would have a stronger impact on production than in the previous case. In this scenario, the pressure gradient in the fracture is greater (Figure 21), which leads to a 14% loss in gas cumulative after 12 months of production, and 8% loss in the 10-year gas recovery.

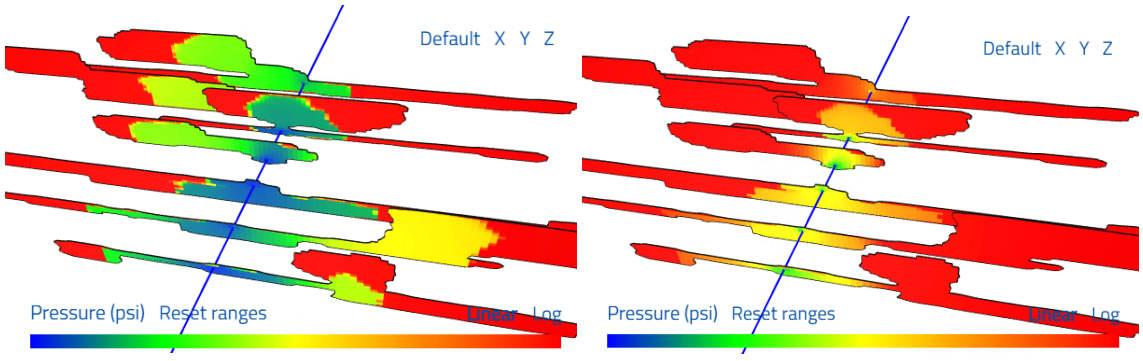

Figure 21: Pressure gradient along the fracture after 6 months of production in the *Extreme* DD case with null rock gamma with (right) and without 10 times lower initial *Fc* (left).

Sensitivity with a combination of adverse effects to proppant production

As discussed in previous sections, certain conditions can amplify the effect of proppant flowback on gas production. Aggressive drawdown management, low initial fracture conductivity, high stress-dependent fracture conductivity decay and absence of stress dependency from rock permeability intensify the detrimental effect of proppant flowback on hydrocarbon recovery. We ran a model that combines all the previous effects in order to quantify gas production losses from proppant flowback under extremely adverse conditions. Again, simulations were conducted with and without allowing proppant to flow back in the model.

The simulated pressure gradient in the fracture is higher than in all previous simulations (Figure 22). Consequently, the gas production was deeply affected after proppant flowback. The model with proppant production recovered 28% less gas in the first year of production, and 20% less gas after 10 years than the case run without proppant production (Figure 22). Figure 23 shows production losses in each individual cluster, reaching up to 25%. It's relevant to point out that this well would have seen minimal proppant flowback if the model had been run normally given its extremely low rates (Figure 16).

Figure 22: Pressure gradient in the fractures in the *Extreme DD* case with null rock gamma, low initial fracture conductivity and high fracture gamma after 3 months of production (left); and gas cumulative after ten years of production in the same model run with (yellow curve) and without (red curve) proppant flowback (right).

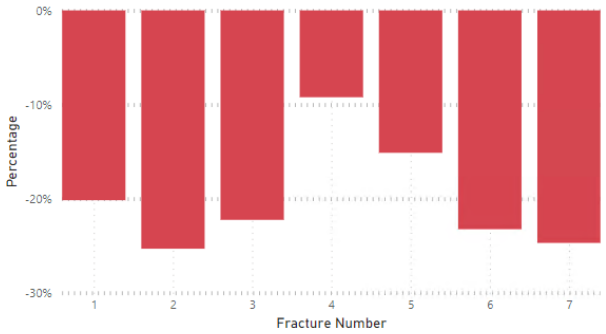

Figure 23: Gas production losses per cluster due to proppant flowback in the *Extreme DD* case with null rock gamma, low initial fracture conductivity and high fracture gamma.

Sensitivity to time-dependent fracture conductivity

Previous works (Duenckel et al., 2017; Pearson et al., 2020) have addressed the existence of time-dependent fracture conductivity damage progressively developing in fractures subjected to closure stress and high temperature. In many cases, this is the only way to explain well production behavior over time. While the base model of *Well 1* reproduces the first year of production reasonably well, it overestimates the expected EUR when compared to the value estimated by the operator based on analogous wells with longer production times in the field. The inclusion of stress-dependent permeability, even if applied both to the rock and the fractures, is not enough to explain the high initial well productivity and its progressive substantial drop with time. The simplest way to account for a higher long-term decay in production would

be to define a smaller volume in place in the model than estimated through petrophysical analysis. However, the operator extracted cores near the wellbore to come up with the values provided, therefore porosity values come from a reliable technique. Additionally, build-ups consistently show strong pressure recoveries of 70 - 80% of the initial pressure after one year of production. If the estimated volume was indeed overestimated, it would not be possible to observe such pressure recoveries. Time-dependent fracture conductivity is a plausible explanation that accounts for initial high productivity, its sustained decline and the substantial pressure recoveries observed during build-ups in the field (Figure 24).

Time-dependent fracture conductivity damage is modeled in ResFrac by a 'rate constant' that defines the decay rate of fracture conductivity over time with a pseudo-logarithmic relationship (McClure et al. 2022). Therefore, we incorporated a reasonable degree of time-dependent conductivity damage into the model (rate constant equal to 0.0007 days^{-1}), such that the forecast became more consistent with the operator's projections. Since this mostly affects late-time production, it did not distort the history-matched period in the model. Figure 25 compares the pressure gradient after 24 months of production in cases with and without time-dependent conductivity damage. It shows that the pressure gradient is significantly greater in the latter case due to the progressive proppant pack permeability reduction.

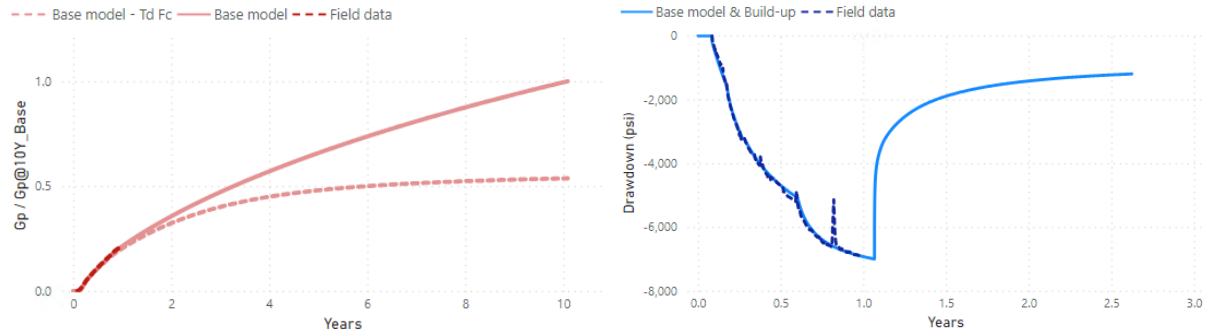

Figure 24: Simulated gas production cumulative with and without time-dependent conductivity damage in the base model for *Well 1* compared with field data (left); and a simulated build-up after one year of production (identical in both models) (right).

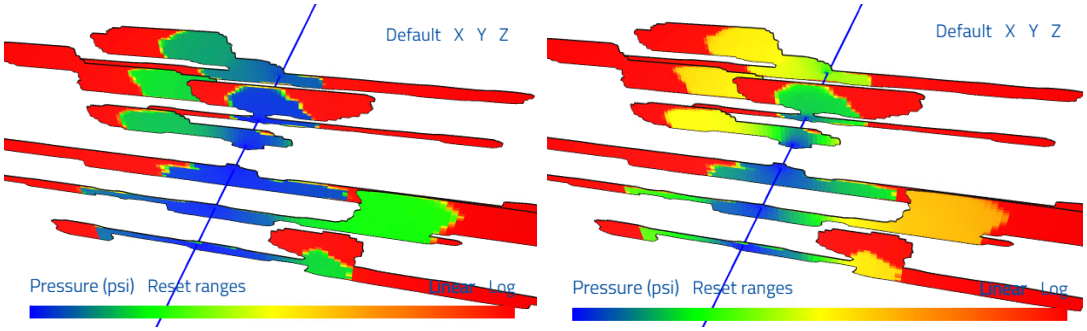

Figure 25: Fracture gradient along the fractures after 24 months of production with *Extreme DD* in the base model (left) and in the base model with time-dependent conductivity (right).

We ran a sensitivity analysis on drawdown with time dependent fracture conductivity. The same drawdown strategies tested for *Well 1* were adopted for comparison. Since gas rates begin to diverge noticeably between cases with and without time-dependent conductivity after 1 year and a half, proppant production was almost identical to the results from the base simulations illustrated in Figure 8. The intermediate drawdown simulations exhibit greater gas recovery, while the conservative and extreme cases have the worst performing EURs. This is explained by a series of juxtaposed effects. The inclusion of time dependent conductivity makes early-time production more important, because at later times the well loses productivity regardless of proppant or gas cumulative. However, while more aggressive drawdown strategies accumulate more hydrocarbon production in the first months, these also result in greater proppant production and fracture conductivity reduction. This is why intermediate drawdown cases recover more gas in the end.

Relative production losses due to proppant flowback range from 0% to 9%, reaching its peak in the extreme drawdown case.

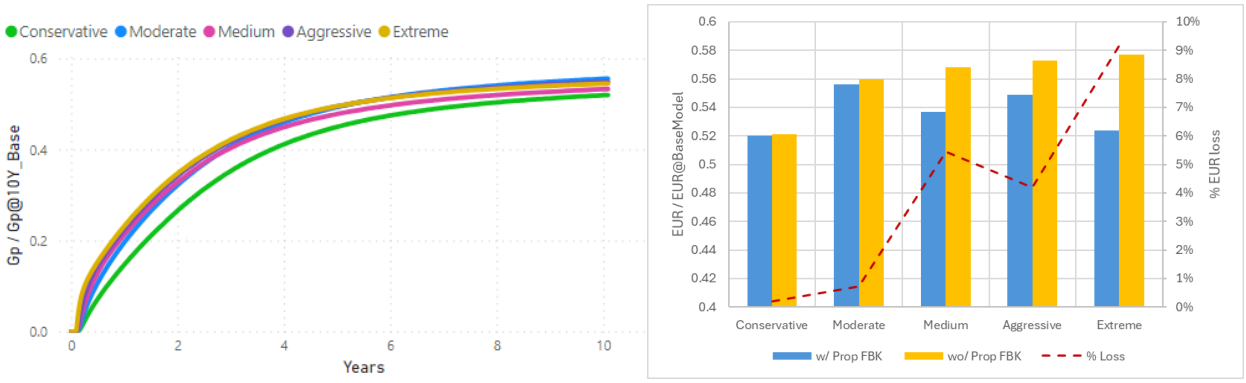

Figure 26: On the left, gas cumulative production curves by case in the sensibility analysis with time-dependent fracture conductivity damage; on the right, gas cumulative after 10 years of production (EUR) by drawdown scenario for *Well 1* with and without accounting for proppant flowback (bars), and production losses due to proppant flowback (dashed line).

Summary of Results

Table 1 summarizes the results presented in the previous sections. In all cases apart from the sensitivity with time-dependent fracture conductivity damage, the relative production losses due to proppant flowback are more significant in the first year than after ten years of production. The addition of mechanisms that increase the pressure gradient along the fracture into the model lead to greater gas production losses due to proppant flowback. Lower initial fracture conductivity, higher stress dependence of the proppant pack permeability and absence of stress dependence on rock permeability gamma increase gas production losses associated with aperture reduction after proppant mass production. Time-dependent fracture conductivity damage also increases production losses after proppant flowback, but its impact is greater in the long term than at early times.

Cases Summary		Conservative	Moderate	Medium	Aggressive	Extreme
Base model	Gp (10yr)	0.97	1.00	1.00	1.00	1.00
	% Loss 1Y	NA	0.0%	NA	NA	1.6%
	% Loss 10Y	NA	0.0%	NA	NA	0.6%
Low initial Fc	Gp (10yr)	NA	0.84	NA	NA	0.83
	% Loss 1Y	NA	3.5%	NA	NA	11.1%
	% Loss 10Y	NA	1.9%	NA	NA	4.4%
High Fc gamma	Gp (10yr)	NA	0.59	NA	NA	0.57
	% Loss 1Y	NA	3.2%	NA	NA	11.9%
	% Loss 10Y	NA	2.5%	NA	NA	5.9%
No rock gamma + High initial Fc	Gp (10yr)	NA	1.49	NA	NA	1.50
	% Loss 1Y	NA	0.0%	NA	NA	2.8%
	% Loss 10Y	NA	0.1%	NA	NA	1.0%
No rock gamma + Low initial Fc	Gp (10yr)	NA	1.10	NA	NA	1.07
	% Loss 1Y	NA	3.6%	NA	NA	16.4%
	% Loss 10Y	NA	3.4%	NA	NA	7.3%
No rock gamma + Low initial Fc + High Fc gamma	Gp (10yr)	NA	0.29	NA	NA	0.25
	% Loss 1Y	NA	9.4%	NA	NA	26.9%
	% Loss 10Y	NA	9.2%	NA	NA	20.8%
Time dependent Fc	Gp (10yr)	0.52	0.56	0.54	0.55	0.52
	% Loss 1Y	0.0%	0.5%	2.2%	1.3%	2.1%
	% Loss 10Y	0.2%	0.7%	5.5%	4.2%	9.2%

Table 1: Summary of results from sensitivities carried out in *Well 1*. It describes the gas cumulative after 10 years normalized by the 10-year cumulative of the *Moderate DD* case in each well, and the relative production loss due to proppant flowback after 1 and 10 years.

This study accounts for productivity damage due to proppant flowback, stress-dependent rock permeability and fracture conductivity, and time-dependent fracture conductivity. There are a variety of additional damage mechanisms to well production caused by excessive drawdown that are not captured in this work. Suarez-Rivera et al. (2011) suggested that excessive drawdown along the fracture face could exceed the tensile strength of the formation and trigger solid production from the formation. They noted that this could result in plugging of the propped fracture and in fracture conductivity losses. Proppant crushing and proppant embedment are also impacted by stress effects (Bandara et al., 2021) and can be accelerated by more aggressive drawdown strategies. Production losses have been reported in the past due to aggressive drawdown strategies, not necessarily associated with proppant flowback. Rojas and Lerza (2018) noticed well productivity decrease in unconventional oil wells producing from Vaca Muerta Fm. with increasing drawdown and attributed this to 'geomechanical effects.' Thus, this work is not presented as a guideline on drawdown management.

Conclusions

The following conclusions derive from the present study:

1. We tested and validated in ResFrac the semi-mechanistic model by Canon et al. (2003) to predict proppant flowback triggering and implemented empirical equations to quantify proppant flowback. Numerical models of two unconventional wells were integrally matched to reproduce field observations using dynamic curves of gas, water, and proppant mass production for the first time.
2. Simulations support that proppant mass production increases with increasing drawdown. The extreme drawdown case simulated in the most proppant-producing well returned 4% of the total proppant pumped during stimulation.
3. There is no correlation between gas production and proppant production between clusters. Proppant pack instability is influenced mostly by fracture aperture, while gas production strongly depends on fracture area.
4. Simulations showed that proppant production does not seem to have a detrimental effect on gas production in the modeled wells, even at extremely aggressive drawdown managements. Fractures remained propped close to the wellbore and despite near-wellbore aperture reduction of up to 7 times, the pressure gradient in the fracture remained negligible compared to the reservoir.
5. The base case was re-modeled to evaluate results in a more adverse scenario by incorporating lower initial fracture conductivity, absence of stress-dependence on rock permeability and higher stress-dependence on fracture conductivity. Results in the most adverse case showed losses of up to 27% in the first-year gas cumulative and 21% losses in the 10-year gas cumulative due to proppant flowback. Total loss of hydrocarbon production associated only with proppant flowback seems unlikely in unconventional wells.
6. At conservative drawdowns, proppant flows back from only a selection of clusters in the model, which do not necessarily correlate with the most hydrocarbon producing clusters. As drawdown becomes more aggressive, more clusters contribute to total proppant production.
7. In most cases in which proppant flowback damages production, the impact is stronger in early times and diminishes at late times as matrix flow capacity decreases with a growing radius of investigation.
8. Proppant mass rates can be used as an additional constraint for the model to narrow down the space of solutions for fracture geometry, particularly for fracture aperture and proppant concentration near the wellbore.
9. In cases affected by time-dependent fracture conductivity damage, production losses due to proppant flowback become more significant, reaching up to 9% loss in 10-year gas cumulative. Intermediate drawdown cases performed better in the simulations since early-time production becomes more relevant for the final recovery of the well and these did not flow back a critical amount of proppant to significantly decrease gas production.

10. Future work should investigate which variations in stimulation design could fully prevent proppant flowback.

References

Agarwal, R.G., Carter, R.D., and Pollock, C.B. 1979. Evaluation and Performance Prediction of Low-Permeability Gas Wells Stimulated by Massive Hydraulic Fracturing." J Pet Technol 31 (1979): 362–372.

Almasoodi, M. & Andrews, T. & Johnston, C., Singh, A. and McClure, M. 2023. A new method for interpreting well-to-well interference tests and quantifying the magnitude of production impact: Theory and applications in a multi-basin case study. arXiv:2302.01968.

Asgian, M.I., Cundall, P.A., and B.H.G. Brady. 1995. The Mechanical Stability of Propped Hydraulic Fractures: A Numerical Study. J Pet Technol 47 (1995): 203–208.

Bandara, K.M., Ranjith, P.G., Rathnaweera, T.D., Wanniarachchi, W.A.M., Yang, S.Q. Crushing and embedment of proppant packs under cyclic loading: An insight to enhanced unconventional oil/gas recovery. Geoscience Frontiers 12 (6) 2021 100970, ISSN: 1674-9871.

Benish, T. G., Brown, J. S, Chhatre, S. S., et al. 2024. Evaluation of Completion Designs and Fracture Heterogeneity via an Instrumented Slant Monitor Well. Presented at the SPE Hydraulic Fracturing Technology Conference and Exhibition, The Woodlands, Texas, USA, February 2024. SPE-217825-MS.

Canon, J., Romero, D., Pham, T., and Valko, P. 2003. Avoiding Proppant Flowback in Tight-Gas Completions with Improved Fracture Design. Presented in the SPE Annual Technical Conference and Exhibition, Denver, Colorado. SPE 84310.

Chuprakov, D. Belyakova, L. Iuldasheva, A. et al. 2020. Proppant Flowback: Can We Mitigate the Risk? Presented at the SPE Hydraulic Fracturing Technology Conference and Exhibition held in The Woodlands, Texas. SPE-199748-MS.

Cinco L., H., Samaniego, F., and Dominguez, N. 1978. Transient Pressure Behavior for a Well with a Finite-Conductivity Vertical Fracture. SPE J. 18 (1978): 253–264.

Duenckel, R. J., Barree, R. D., Drylie, S., O'Connell, L. G. et al. 2017. Proppants - What 30 Years of Study Has Taught Us. Presented at the Annual Technical Conference and Exhibition, San Antonio, TX. SPE-187451-MS.

Goel, N. and Shah, S. N. 1999. Experimental Investigation of Proppant Flowback Phenomena Using a Large Scale Fracturing Simulator. Presented at The SPE Annual Technical Conference and Exhibition, Houston, TX. SPE-56880-MS.

Gray, H.E. 1978. Vertical flow correlation in gas wells. Vol. User's Manual for API 14B Surface Controlled Subsurface Safety Valve Sizing Computer Program, 2n Edition, (Appendix B), American Petroleum Institute, Dallas, TX(Reprint).

Guo, S., Wang, B., Li, Y., Hao, H., Zhang, M. and Liang, T. 2022. Impacts of Proppant Flowback on Fracture Conductivity in Different Fracturing Fluids and Flowback Conditions. ACS Omega 2022 7 (8), 6682-6690.

Heller R, Vermylen J, and Zoback M: Experimental Investigation of matrix permeability of gas shales. The American Association of Petroleum Geologists Bulletin 98 (5) 2014: 975–995.

Karantinos, E. Sharma, M. M., Ayoub, J.A., Parlar, M., and Rajesh A. 2015. A General Method for the Selection of an Optimum Choke Management Strategy. SPE-174196-MS.

Karantinos, E., Sharma, M., Ayoub, J., Parlar, M. and Rajesh, A. 2015. Choke-Management Strategies for Hydraulically Fractured Wells and Frac-Pack Completions in Vertical Wells. SPE 178973.

Krauss, E. D., Mays., D. C. 2014. Modification of the Kozeny-Carman equation to quantify formation damage by fines in clean, unconsolidated porous media. SPE Reservoir Evaluation & Engineering 17 (4): 466-472.

Kwon, O., Kronenberg, A. K., Gangi, A. F., and Johnson, B. 2001. Permeability of Wilcox shale and its effective pressure law. J. Geophys. Res. 106(B9): 19339–19353.

Liang, Y., Meier, H., Srinivasan, K., et al. 2022. Accelerating Development Optimization in the Bakken Using an Integrated Fracture Diagnostic Pilot. Paper presented at the SPE/AAPG/SEG Unconventional Resources Technology Conference, Houston, Texas, USA. URTEC-3719696.

McClure, M., Fowler, G., Hewson, C., and Kang, C. 2023. The A to Z Guide to Accelerating Continuous Improvement with ResFrac. 6th version, March 2023.

McClure, M., Kang, C., Hewson, C., Medam, S., Dontsov, E., and Singh, A. 2022. ResFrac Technical Writeup, September 30, 2022 Update.

McClure, M., Picone, M., Fowler, G., Ratcliff, D., Kang, C., Medam, S., and Frantz, J. 2020. Nuances and frequently asked questions in field-scale hydraulic fracture modeling. Presented at the Hydrauic Fracturing Technology Conference, The Woodlands, TX. SPE 199726-MS.

McGinley, M., Zhu, D., and Hill, A.D. 2015. The Effects of Fracture Orientation and Elastic Property Anisotropy on Hydraulic Fracture Conductivity in the Marcellus Shale. Presented at the SPE Annual Technical Conference and Exhibition, Houston, Texas, USA. SPE-174870-MS.

Pandey, V. 2023. Proppant Flowback Prevention and Control by Analysis of Early Time Well Production Data. Presented at the 2023 SPE Annual Technical Conference and Exhibition held in San Antonio, Texas. SPE-214959-MS.

Parker, M., Weaver, J., and Van Batenburg, D. 1999. Understanding Proppant Flowback. Presented at the SPE Annual Technical Conference and Exhibition, Houston, Texas. SPE-56726-MS.

Pearson, C., Garrett, F., Stribling, K., McChesney, J., McClure, M. et al. 2020. Near-Wellbore Deposition of High Conductivity Proppant to Improve Effective Fracture Conductivity and Productivity of Horizontal Well Stimulations. Presented at the SPE Annual Technical Conference and Exhibition. SPE-201641-MS.

Raterman, K., Liu, Y., and Warren, L. 2019. Analysis of a Drained Rock Volume: An Eagle Ford Example. Presented at the SPE/AAPG/SEG Unconventional Resources Technology Conference, Denver, Colorado. URTEC-2019-263-MS.

Rojas, D., and Lerza, A. Horizontal Well Productivity Enhancement through Drawdown Management Approach in Vaca Muerta Shale. Presented at the SPE Canada Unconventional Resources Conference held in Calgary, Alberta, Canada, 13-14 March 2018. SPE-189822-MS

Shor, R. J., and Sharma, M. M., 2014. Reducing Proppant Flowback from Fractures: Factors Affecting the Maximum Flowback Rate. SPE 168649.

Suarez-Rivera, R. Deenadayalu, C. Chertov, M. et al. 2011. Improving Horizontal Completions on Heterogeneous Tight Shales. Presented at the Canadian Unconventional Resources Conference held in Calgary, Alberta, Canada. CSUG/SPE 146998.

US Energy Information Administration (EIA). 2013. Technically Recoverable Shale Oil and Shale Gas Resources: An Assessment of 137 Shale Formations in 41 Countries Outside the United States. https://www.eia.gov/analysis/studies/worldshalegas/

Wattenbarger, R. A., El-Banbi, A. H., Villegas, M. E., and Maggard, J. B. 1998. Production Analysis of Linear Flow Into Fractured Tight Gas Wells. Presented at the SPE Rocky Mountain Regional/Low-Permeability Reservoirs Symposium, Denver, Colorado. SPE-39931-MS.

Zhang, Z. and Guo, B. 2016. The Critical Flow Back Velocity in Hydraulic-Fracturing Shale Gas Wells. International Journal of Engineering Research and Applications 6 (2): 7–11.

Appendix

Each fracture block in the model has its own proppant pack permeability and aperture, thus its own conductivity at each time step. This spatial distribution of fracture conductivities cannot be directly utilized to estimate *FCD* (Figure A-1). Thus, it is necessary to compute an effective fracture conductivity for each cluster to analyze the evolution of dimensionless fracture conductivity with stress and time in the simulations. We derived expressions for equivalent fracture conductivity through Darcy's equation for linear flow in parallel and in series to estimate the effective conductivity of the fracture. The blocks distribution in a fracture can be organized in terms of rows and columns. We filtered all elements with fracture conductivity below 0.1 mD-ft to guarantee that the effective conductivity would not be affected by closure of unpropped fractures and would remain greater than zero. Therefore, the solved average conductivity represents only the conductive portion of the fracture area, which is mostly propped. First, we solve for the effective fracture conductivity of the sum of blocks in all rows for each column with the solution for linear flow in parallel by Darcy's law:

$$Fc_i\, H_{T_i} = \sum F_{c_{i,j}} H_{i,j} \tag{A-1}$$

Where Fc_i is the equivalent fracture conductivity of each column of elements, and H_{T_i} is the total height of the column of elements. The only exception is the last column, where the fluid in most elements can only flow in a vertical direction towards the block connected to the well (Figure A-1). For this reason, the product of conductivity times height for this column is left equal to the conductivity times height of the block connected to the well. In this way, this block can act as a 'choke' for the whole fracture's effective conductivity. Once the effective conductivity for each column of blocks is computed, we calculate the effective fracture conductivity of the whole fracture by solving for linear flow in series:

$$Fc_{ef} = \frac{\frac{L_T}{H_{ef}}}{\sum \frac{L_{T_i}}{F_{c_i} H_{T_i}}} \tag{A-2}$$

Eq. A-2 weighs the conductivity of each block on element length (L_{T_i}), while H_{ef} represents the average height of the conductive portion of the whole fracture. This comes from dividing the sum of all conductive element areas by the total length of all columns with conductive elements. Eq. A-2 results in an effective fracture conductivity of the whole fracture (Fc_{ef}). *FCD* is then given by the ratio of the effective fracture conductivity and the product of total half-length (x_f) with matrix permeability (k_m):

$$FCD = \frac{F_{cef}}{k_m\, x_f} \tag{A-3}$$

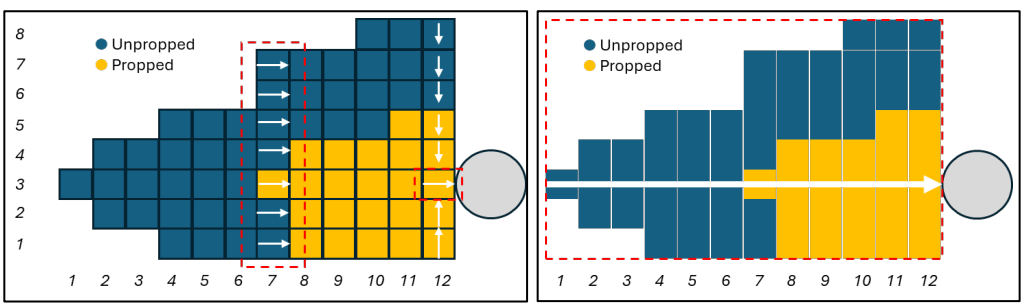

Figure A-1: Scheme of a fracture in the model, each block is a different element with associated length, height, proppant pack permeability and aperture. Arrows represent the direction of the fluid flow during production.